Synthesis and Investigation of Electrical and Magnetic Properties of Cobalt doped Barium Monoferrite for High Frequency Applications

By

Tahseen Arshad

School of Chemical and Materials Engineering

National University of Sciences and Technology

2021

Synthesis and Investigation of Electrical and Magnetic Properties of Cobalt doped Barium Monoferrite for High Frequency Applications

Name: Tahseen Arshad

Registration No: Fall 2018-NSE 06, 00000273734

This thesis is submitted as a partial fulfillment of the requirements for the degree of

Master of Science in Nanoscience and Engineering

Supervisor Name: Dr. Iftikhar Hussain Gul

School of Chemical and Materials Engineering (SCME)

National University of Sciences and Technology (NUST)

H-12 Islamabad, Pakistan

April,2021

Dedication

With deep sense of gratitude, humbleness, and warmest affection I would like to dedicate this thesis to my family and colleagues for their continuous help and support.

Acknowledgements

All praise and gratitude belong to *Allah Almighty* for giving me the strength, ability, and opportunity to understand, learn and complete this research work.

Special appreciation goes to my research supervisor Dr. Iftikhar Hussain Gul for his precious time and constant support throughout my work. This research could not have been possible without his invaluable guidance, constructive comments, and suggestions throughout the experimental and thesis work.

I am also thankful to my family, friends and colleagues for their moral support, kindness ,and care. Thank you all very much.

Regards

Tahseen Arshad

Abstract

Spinel structures are lately being explored widely because of their crucial applications in electromagnetic absorbing materials, high frequency devices, memory devices, photocatalysts and catalysts. The exponentially remarkable electrical and magnetic properties of ferrites have always been of prime interest which leads to their extensive commercial use. In present study barium monoferrite with formula $Ba_{1-x}Co_xFe_2O_4$ where x= 0.00 ,0.20 ,0.35 ,0.50 ,0.75, 1.00 has been prepared through sol gel auto-combustion method. Stoichiometric ratios of citric acid, barium, cobalt and iron nitrates along with ammonia solution for maintaining solution's pH were used for the preparation of samples. Samples were calcinated at 800 °C for 4 hours. Sample characterization was made using X-Ray Diffraction analysis (XRD), Fourier transform infrared spectroscopy (FTIR). Electrical and magnetic behaviors were analyzed through Vibrating sample magnetometer and RF impedance analyzer. Formation of $Ba_{1-x}Co_xFe_2O_4$ was confirmed using XRD. Crystallite sizes were calculated through Debye Scherer formula which lie in the range (26-40)±5 nm. Octahedral and tetrahedral band positions were confirmed using FTIR data. Room temperature frequency dependence of dielectric properties were observed to be enhanced till certain concentrations, then a decreasing trend was observed. Dielectric constant was increased from 5.7 to 16.7 for x=0.35 at 1MHz. The magnetic properties of prepared samples showed an increase in saturation magnetization from 2.69 emu/g at x=0.00 to 84.8 emu/g at x=1.00. A decrease in magnetic coercivity is observed with increase in concentration. The high and quite comparable values of dielectric constant make this material suitable for use as a microwave absorbing paint as well as a promising Electromagnetic Interference (EMI) shielding material.

Table of Contents

List of Figures

List of Tables

List of Abbreviations

Acronym	Abbreviations
NPs	Nano Particles
NCs	Nano Composites
XRD	X-Ray Diffraction
FTIR	Fourier Transform Infrared
SEM	Scanning-Electron-Microscopy
VSM	Vibrating Sample Magnetometer

CHAPTER 1

History of Ferrites

Centuries ago, the discovery of stones that would attract iron, led the history of ferrites. The mineral got the name "magnetite". Magnetite's early administration was as 'Lodestones' used by early navigators to pinpoint magnetic North. In 1819 Hans Christian Oersted noted that magnetic compass needle was affected by the electric current in a wire. With further donative by Faraday, Maxwell, Hertz and many others, the new science of electromagnetism was developed. Ferrites are primarily used in three main domains of electronics: low level applications, power applications, and Electro-Magnetic Interference (EMI) suppression. The span of utilization of ferrites in electronic circuitry is continuously flourishing. Ferrite compounds serve as an excellent material for innovative and experimental applications because of their wide range of possible geometries, cost effectiveness as compared to other materials and constantly improving properties.

1.1 INTRODUCTION

The importance of ferromagnetic materials, particularly Spinel Ferrite, have led recent researchers to investigate their chemical and physical characteristics in depth. Materials such as spinel ferrite have vast potentials of use in technology and scientific research and progress, which further forces the researchers to get to know about their properties to produce beneficial instruments and equipment to advance in technology. These materials are of great importance with a wide range of applications in drug delivery, chemical sensors, MRI imaging, Spintronics and many other energy storing devices. [1] [2] [3] [4]. Spinel ferrites have valuable properties such as dielectric and magnetic characteristics along with resistivity, which makes them a brilliant choice for usage in electronic industry too, where materials can be used as antennas, convertors, switching devices, transformer cores, radio frequency filter coils, transformer cores and various magnetic storage media devices. [5] [6] [7] [8].

Atom is the building block of everything present in universe, which consists of a nucleus surrounded by moving electrons in particular orbits. Along with orbital motion, electrons spin around their own axis. Moving electrons produce small currents and those changing currents produce a magnetic field whose moments align along axis of rotation. Magnetic moments produced due to spin of electrons can have an up or down direction depending upon spin. Therefore, magnetic moments of completely filled orbitals are zero. Now a day, every kind of machine ranging from simple household machine to heavy industrial machine employ magnets. To clearly understand the concept of magnetism the concept of dipole is very important. The dipole can be considered as a basic source of magnetism. Magnetism can be considered as the ability of the material to respond a magnetic field. Magnetic field has an attractive effect on some materials and on the other materials it can have repulsive effect. Some materials show no response when magnetic field is applied. Magnetic permeability μ and magnetic susceptibility χ relate magnetizing force (H), magnetic flux density (B) and magnetization (M) to each other.

1.2 Classification of Ferrites

The behavior of a material varies depending upon variation of internal and external flux along with magnetization and magnetic induction caused by the applied field. This difference in behavior can be attributed to many factors like atomic or molecular structure or collective magnetic moment of the entire atom. The spin and orbital motions of electrons considerably affect the magnetic moments. Also, the spin and orbital motion is changed by magnetic field applied externally. Magnetic moments of some materials align in direction of external magnetic field and some against it. In atoms consisting of paired electron, magnetic moments cancel each other due to opposite spins. While atoms having unpaired electrons have some value of net magnetic field. These characteristics dictate the behavior of material in reaction to magnetic field and depending upon these behaviors, magnetic materials are divided into following branches:

1. Para Magnetism
2. Dia Magnetism

3. Ferro/Ferrimagnetism
4. Super-Para Magnetism
5. AntiFerromagnetism

1.2.1 Para Magnetism

Para magnetism arises due to incomplete cancelation of orbital and spin magnetic moments. Internal induced magnetic fields are formed in direction of applied magnetic fields by materials that are feebly attracted by external magnetic field. When no magnetic field is applied the dipoles are randomly oriented in domains. This will result in zero net magnetization. The net magnetization is gained by applying magnetic field. The magnetic field will position the magnetic moments in direction of field, this will result in some net magnetization. On removal of external magnetic field, moments realign themselves as shown in figure 1

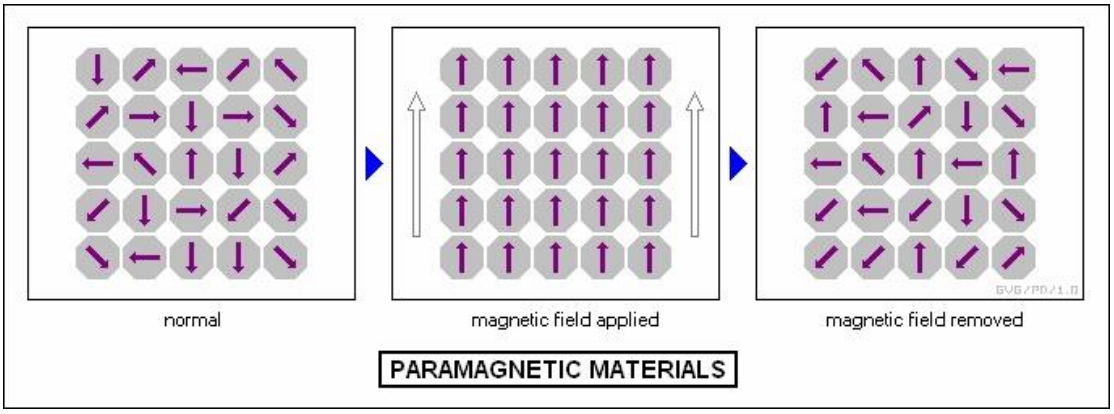

Figure 1. Atomic Dipoles Configuration for Paramagnetic Materials [9]

1.2.2 Dia Magnetism

The electron's orbital motion in presence of magnetic field will give rise to diamagnetism. The diamagnetism exists when the net magnetic moment of atom is zero. The atom's orbital motion produces a magnetic field that opposes the applied magnetic field. This is explained by negative susceptibility. The movement of material is towards the place where the strength of magnetic field is weak.

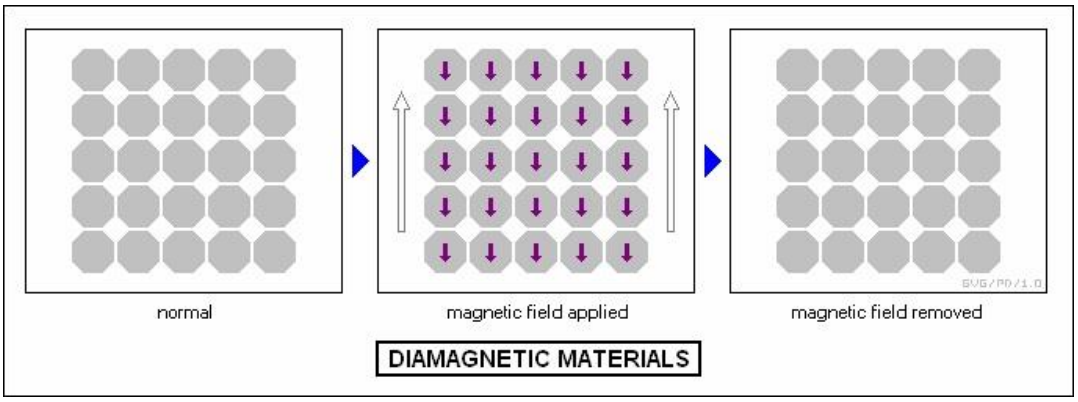

Figure 2. Atomic Dipole Ordering of Dia Magnetic Materials [9]

1.2.3 Ferro Magnetism and Ferrimagnetism

In the view of classical theory, the effect of Ferromagnetism can be described as a presence of field inside a material that allows and helps the magnetic moments of atoms to interact and align parallel to each other. The inbuilt filed is ample to magnetize the material to saturation. In their elemental form only iron, cobalt and nickel show ferromagnetic behavior at and above room temperature. With the increase in temperature the alignment of atomic magnetic moment mostly decreases, and material becomes paramagnetic at high temperatures. This transitional temperature is called Curie temperature. Mutual interaction of spin of domains creates the basis of this permanent magnetic moment in ferromagnetic. Domains have spins aligned in same directions. Where the incomplete cancellation of dipole moment causes a lower permanent magnetization in ferrimagnetic materials. Sum of domain's magnetization make up the macroscopic magnetization. Generally ferromagnetic materials are ionic solid i.e. they are electrically non-conductor whereas the ferrimagnetic materials are metals i.e. conductors

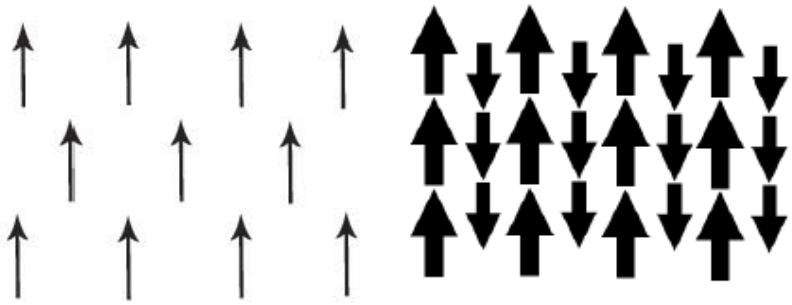

Figure 3. Atomic Dipole Ordering of Ferro and Ferri Magnetism [9]

1.2.4 Anti-Ferromagnetism

The phenomena of anti-ferromagnetism are same as ferromagnetism. But the difference in this case is interaction of magnetic moments propagates the antiparallel alignment of them. All magnetic moments cancel the effect of each other and in result behave as a diamagnetic material. Chromium is the only material which shows this kind of behavior at room temperature. This behavior is also temperature dependent. By increasing the temperature increase in thermal movements changes the material to paramagnetic material above transition temperature. In this case this temperature is knows as Neel temperature.

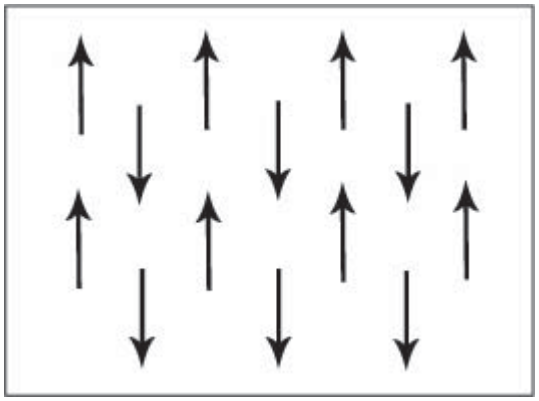

Figure 4. Atomic Dipole Ordering of Anti-Ferromagnetism [10]

1.2.5 Super-Para Magnetism

The super Para magnetism arises when a material is subjected to temperature less than curie temperature. This will result in the alignment of neighboring atom's magnetic moments.

1.3 Ferrites Overview

Ferrite is a term generally used to mention a metal oxide in which main component of crystal structure is iron oxide. Ferrites have a big number of applications including applications in transformer cores and permanent magnets because of its magnetic nature. The unique ability to hinder the production of eddy currents due to their highly resistive nature makes them useful in applications involving high frequencies. They show high electrical resistivity. On basis of hysteresis, ferrites have two types, soft ferrites and hard ferrites.

1.3.1 Hard Ferrites

Hard ferrites are also termed as ceramic ferrites. They show large coercivity values, so they take more time to demagnetize entirely. They have a high value of magnetic permeability. Hard ferrites are usually made up of strontium, iron and barium oxides. They are less expensive because materials required for their preparation are easily available. Their low cost makes them applicable in household items [9] . Ferrites of cobalt and strontium are examples of hard ferrites.

1.3.2 Soft Ferrites

Soft ferrites are the type if ferrites which can be magnetized and demagnetized easily by the application and removal of applied field. They can only remain magnetized when they are in the influence of magnetic field. Soft ferrites have low values of coercivity. They also show low energy dissipation values during magnetization. Their appearance is usually dark in color e.g. gray or black. Soft ferrites are usually brittle and hard. The value of resistivity is also high. For soft ferrites the value of hysteresis loop and coercivity is very low. This implies that these materials can reverse magnetization directions easily without

losing any or much energy [10] .They are applicable in inductors and transformer cores so that energy losses can be minimized. Some examples of soft ferrites include zinc and nickel ferrite [9] .

An ideal ferrite would have

- Low value coercivity
- Large value of saturation magnetization
- Zero value of remanence
- Zero hysteresis loss value
- Large permeability [11]

1.4 Composition of Ferrites

The general chemical formula for ferrites is $M^{+2}Fe_2^{+3}O_4^{-2}$ where M is metal divalent ion for example:

- Cobalt ion (Co^{+2})
- Nickel ion (Ni^{+2})
- Magnesium ion (Mg^{+2})
- Copper ion (Cu^{+2})
- Zinc ion (Zn^{+2})

A combination of mixed ferrites with equivalent valency which are known as mixed ferrites is also possible.

1.5 Classes of Ferrites

Ferrites are divided into the following three types on the basis of their structure:

- Spinel Ferrites
- Hexagonal Ferrites
- Garnet Ferrites

1.5.1 Garnet Ferrites

In 1957 Galileo discovered garnets**.** General formula for garnets is $M_3Fe_5O_{12}$ and they occupy a cubic structure. Where M represents trivalent ion of rare earth metals. Some of the examples of trivalent ions of rare earth metals are Y, Dy, Gd etc. Garnets generally fall in the category of hard materials.

1.5.2 Hexagonal Ferrites

Hexagonal ferrites are made up of Fe, O and divalent ions with chemical formula: $MFe_{12}O_{19,}$ where M is a divalent ion usually Ba, Sr, or Pb (barium, strontium or lead).
This structure resembles the spinel structure where the oxygen lattice consisted of a series of hexagonal layers of oxygen lying perpendicular to the (111) direction as in FCC. Their structures are complex which can be described as hexagonal lattice with additional (vertical) c-axis. Hexagonal ferrites mostly magnetize along this axis easily and their magnetization direction cannot be changed to other axes easily. Hexagonal lattice consists of three different lattice sites which are occupied by metal ions.

- Tetrahedral site
- Octahedral site
- Trigonal-bi-pyramid

Each side of metal ions is surrounded by 6 oxygen ions. Their crystal as well as magnetic structure of hexagonal ferrites are remarkably complex and cannot be easily described.

1.5.3 Spinel Ferrites

Like hexagonal ferrites spinel ferrites are also made up of Fe, O and divalent cations and their chemical formula is MFe_2O_4. Here M stands for divalent cations. Then example of divalent cations includes nickel Ni^{+2}, copper Cu^{+2}, zinc Zn^{+2}, cobalt Co^{+2} etc. Among all the types of ferrite, spinal ferrites have comparatively simple structure. The number of oxygen ions present in its unit cell is 32. The arrangement of anions obeys face centered cubic closed packed structure. The two types of sites B and A present between anions are referred as octahedral and tetrahedral sites respectively. The number of oxygen atom surrounding a tetrahedral site is 4. There are 64 tetrahedral sites in a spinal structure. The

cations are present on 8 tetrahedral sites. The number of oxygen atoms surrounding an octahedral site is 6. The number of octahedral sites present in a spinal structure is 32. The anions are present on 16 octahedral sites. The spinal structure is electrically neutral due to presence of A and B sites.

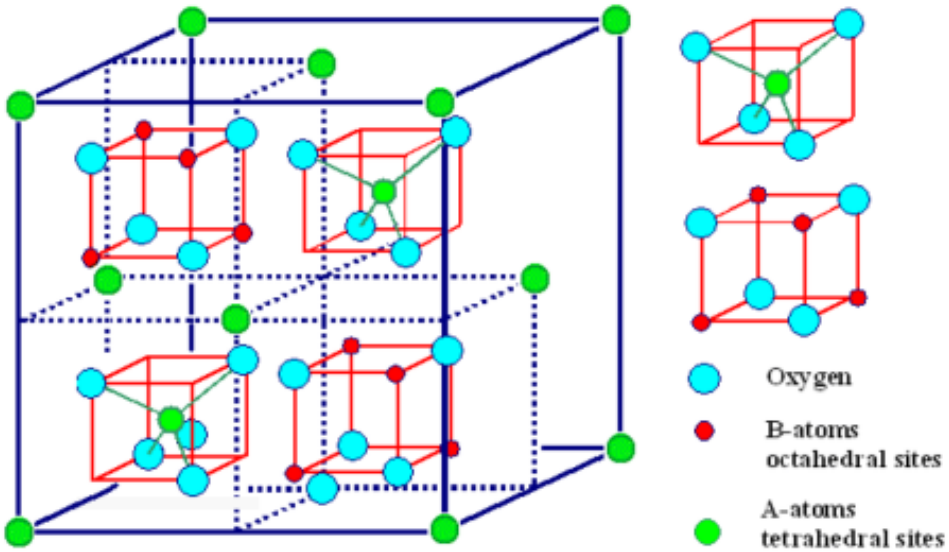

AB_2O_4 **spinel** The red cubes are also contained in the back half of the unit cell

Figure 5. Unit Cell of Spinal Ferrites showing Octahedral and Tetrahedral sites [11]

1.5.3.1 Types of Spinel Ferrites

Spinel structures are of three types:

1. Mixed spinel
2. Inverse spinel
3. Normal spinel

In the case of inverse spinel structures, there are trivalent ions present on both the A site and the B site both while on the site B there are divalent ions too. While in normal spinel structures, A sites have divalent whereas B sites are occupied by trivalent ions. In mixed spinel ferrites, on both the tetrahedral and the octahedral sites there are bivalent ions. The distribution of random spinel ferrites depends upon the process of synthesis and sintering process.

1.6 Cation Distribution

The cationic distribution in spinel ferrites greatly influence magnetic and electrical properties. There is a number of factors that affect the distribution of Fe and the M^{+2} among the tetrahedral and octahedral sites. The cationic distribution can be determined by several methods. Some of them are.

- X-ray diffraction methods [12]
- Magnetic susceptibility measurement
- Infrared absorption spectroscopy [13]
- Mossbauer spectroscopy [14]
- Neutron diffraction method

1.7 Factors Affecting Cationic Distribution

The distribution of cations at tetrahedral and the octahedral sites is affected by:

- Electronic configuration
- Method of preparation
- Ionic radius

1.7.1 Ionic Radius

As we see that the B sites or the octahedral sites have a larger ionic radius then the A or the tetrahedral sites in case of spinel lattice. So large cations like Co^{+2} and Ni^{+2} will prefer occupying the Octahedral sites instead of occupying a smaller tetrahedral site.

1.7.2 The Electronic Configuration

It is a common observation that ions with filled d-shell often have tendency to form sp^3 hybrid orbital and occupy the tetrahedral (A) sites for example Zn^{+2} and Ge^{+4}, whereas the ions with d^3 and s^8 electronic configuration has tendency to form d^3 sp^3 hybrid orbitals and occupy the octahedral sites in spinel structure. For example, Cr^{+3} and Ni^{+2} [15]

1.7.3 Method of Preparation

It is observed that method of preparation can also affect the distribution of cations of octahedral sites and tetrahedral sites. The cationic distribution strongly depends on heat treatment (sintering) of the material. Materials with same composition prepared by two different methods can have different properties.

1.8 Applications of Ferrites

The spinel ferrites have a wide range of applications in different fields. Even after hundreds of research works been done over ferrites, the scientist and technologist are still interested in ferrite materials. The recent interest of the researchers is focused on the ferrites doping. Which can be prepared using various compositions, synthesis routes and with different cationic concentrations which highly affects the properties like electrical, dielectric and magnetic of the material. Ferrites are important magnetic materials and have applications in power conditioning, electromagnetic device, electromagnetic wave absorbers, magnetic inks for bank cards, and recording media etc. Some of the major fields of applications of ferrites are listed below

- Medical diagnostics and treatments
- Drug delivery
- Magnetic shielding
- Magnetic sensors
- Electromagnetic interference suppression
- Pollution control
- High frequency applications

1.9 Objective of This Research

The objectives of this research work are as follows:

- Preparation of $BaFe_2O_4$ single phase spinel nanoparticles using sol gel auto-combustion method.
- Preparation of Co substituted $Ba_{(1-x)}Co_xFe_2O_4$, x = 0.02, 0.35, 0.50, 0.75, 1.00 nanoparticles.
- Material characterization using XRD, FTIR.

- Studying the effects of dopant concentrations on magnetic, dielectric and structural properties.

Chapter 2

Theoretical Review

Nanoparticles are synthesized by two major methods.

1. Bottom Up Approach
2. Top Down Approach

The Top Down Method starts from large structures and subsequently using finer methods forms more smaller and finer structures which includes lithography, ball milling, laser ablation, electro spinning, arc discharge etc. In bottom up approach atoms, molecules and clusters are combined together to form nanoparticles. Examples of bottom up approach are wet chemical synthesis, physical vapor deposition (PVD), chemical vapor deposition (CVD), hydrothermal synthesis, MBE, self-assembly etc. Both techniques have some advantages and disadvantages. In top down approach homogeneity and dimensional controls are difficult to maintain. Significant amount of impurity is always present which cannot be totally diminished. While bottom up approach provides better, cheaper, easier and efficient route for synthesis of nanoparticles.

Nanoparticles can be synthesized by various methods. Every method possesses a separate advantages and disadvantages. The chemical, magnetic and structural properties of prepared nano particle depend greatly upon synthesis technique.

Some of the synthesis methods are:

- Micro emulsion technique.
- Co-precipitation technique.
- Solvothermal technique.
- Hydrothermal technique.
- Gas condensation technique.
- Sono-chemical technique.
- Combustion flame synthesis.
- Sol-gel technique.

At room temperature ferrites manifest unique behavior and hence are used in many device applications. Ferrites show low electrical losses and high DC electrical resistivity. Spinal ferrites are preferred due to chemical stability, excellent magnetic properties, simplified synthesis process, reasonable cost and mechanical hardness [16], [17]. Due to fine electrochemical performance, binary metal oxides are extensively applicable in electrochemical applications, like capacitors [18], the fuel cells [19],Li-ion batteries [20], the solar cells [21]. The electrochemical capacitors employ oxides of transition metals having a spinal crystal structure, as they provide a strong crystalline architecture with diffusion pathways in three dimensions [22] . Presently a variety of spinal and inverse spinal ferrites have been tested for electrochemical capacitors. Electronics and catalysis have been extensively employed transition metal oxides because of their high catalytic activity, environmental accordance, and easy separation [23] [24].

2.1 Chemistry of Sol-gel Synthesis

2.1.1 Introduction

The sol gel synthesis is kind of inorganic polymerization. It was firstly described by Ebelmann in 1864. As in practice, sol-gel synthesis looks a very simple process that it requires just one step to get a required product but at nanoscopic scale it is such a complex technique that it goes through several transformations of different nature before the final result.

Sol consist of colloidal suspension in which solid particles (solute) are dispersed in some liquid medium (solvent). The common precursors mostly used in the synthesis of sol–gel are:

- Inorganic salts (chlorides, nitrates)
- organic compounds

This technique uses the condensation and hydrolysis of metal precursors, which in turn forms a 3-D inorganic network. In ferrites, Colloidal solution is composed of chemicals like metalloids or metals surrounded by ligands, metal nitrates are used commonly in this solution. This process known as hydrolysis, Metal ion (M) attached with hydroxyl ion is produced through the reaction shown below.

$$M(OR)_4 + 4H_2O \rightarrow M(OH)_4 + 4ROH$$

Another scenario is possible where while the material is partially hydrolyzed, the hydrolysis stops:

$$M(OR)_4 + H_2O \rightarrow HO - M(OR)_3 + ROH$$

These molecules can condense by linking together. This process liberates water molecule as shown in reaction below

$$(OR)_3M - OH + HO - M(OR)_3 \rightarrow H_2O + (OR)_3 M - O - M(OR)_3$$

This type of continuous reaction builds large metal containing molecule which is called gel. It contains a continuous solid structure which is amorphous naturally, but it can get crystallized during heat treatment. For the preparation of ferrites, sintering of the prepared samples need to be done at elevated temperatures. A step by step guide of sol-gel auto combustion method is shown below:

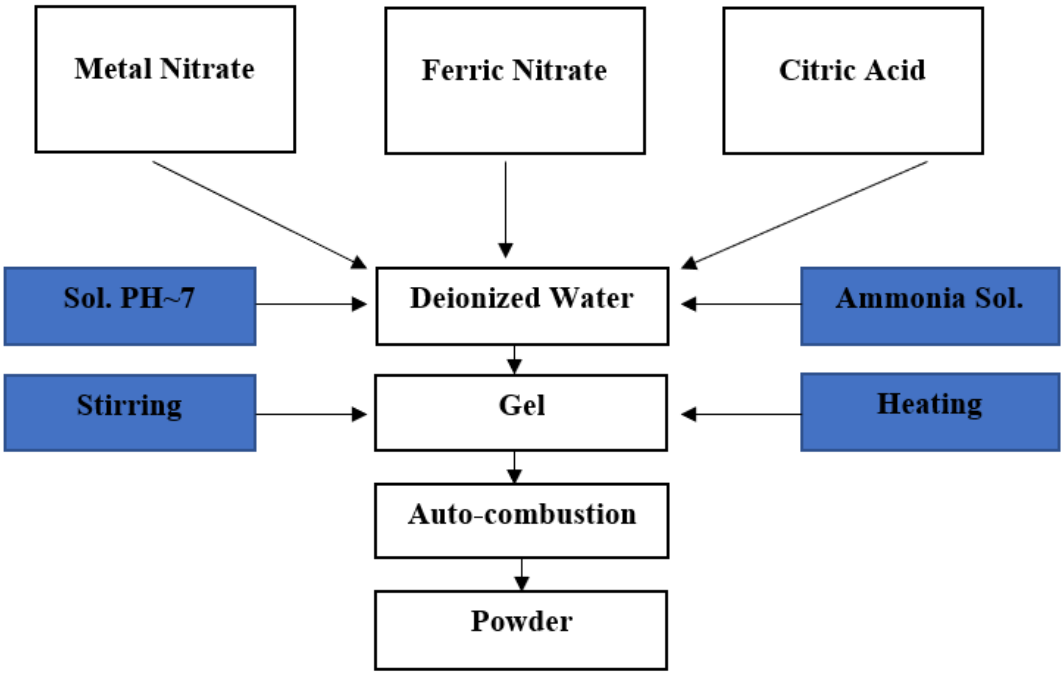

Figure 6. Synthesis of Ferrites Samples Preparation

2.1.2 Effect of Different Parameters on Sol-gel Synthesis

Structure, morphology, and particle size are affected by many factors during preparation. Some of them are:

- Effect of chelating agent
- Effect of pH

2.1.2.1 Effect of Chelating Agent

For the synthesis of powder ferrite nanoparticles metal nitrates and chelating agents e.g. urea, citric acid, glycine, hexamethylenetetramine etc. are used. Mostly the ration of metal nitrates and citric acid is kept at 1:3. The ratio and type of chelating agent greatly influence the magnetic and structural properties, cationic distribution and particle size [25]. The combustion process in each chelating agent occurs differently. In case of hexamethylenetetramine and glycine the process of auto combustion takes only few seconds while for citric and tartaric acid the whole combustion processes takes more than 30 minutes. While in case of urea it took 2-3 minutes to complete auto combustion process [26].

2.1.2.2 Effect of pH

In sol-gel synthesis the pH value of the solution is controlled by ammonia. It catalyzes the process for hydrolysis and then condensation. pH values greatly influence the combustion rate [27]. pH values between (7-8) induce a fast gelation, which is ideal for making small size nanoparticles. While pH values between (2-3) induce low gelation and ideal for making extended network.

2.2 Literature Review

Ferrites are good dielectric materials that's why they have long range of applications for example in microwave devices, targeted drug delivery [28], data storage sensors [29],catalysis [30], core materials and electromagnetic absorbers [31] etc.

R. Dilip prepared $BaFe_2O_4$ spinel-type ferrites for gas sensor applications. VSM results showed the high coercivity value (Hc) to be 3147.39 Oe while the saturation magnetization (Ms) to be 33.15 emu/g. (R) [32]

Samar I. Abdelsalama prepared $BaCo_xFe_{2-x}O_4$ ($0.0 \leq x \leq 0.4$) by solgel auto combustion method with the subsequent heat treatment at 700 °C and 1050 °C. XRD confirmed the formation of pure orthorhombic phase for $x = 0.0 - 0.2$, while few traces of $BaFe_3O_4$ and Ba_2FeO_4 appeared with increasing either *x* or sintering temperature. The unit cell volume was found to be decreasing as the Co content increased ($x \geq 0.2$) for both sintering temperatures. The substitution of non-stoichiometric Co^{+2} ions in mono-barium ferrite results in increasing dielectric loss, dielectric constant and ac conductivity [33].

M.Govindaraj Shalini synthesized cobalt doped barium hexaferrite nanoparticles using modified sol-gel auto-combustion technique and annealed in air for 4 hours at 900 ^{O}C. Reduction in the grain size in $BaFe_{11}CoO_{19}$ sample compared to $BaFe_{12}O_{19}$ sample was observed. Moreover, a magnetization value at 300K for the $BaFe_{12}O_{19}$ was observed to be 60 emu/g which reduced by a considerable 10% after doping in $BaFe_{11}CoO_{19}$ [34].

Kailash Chandra prepared $Mg_xCo_{1-x}Fe_2O_4$ nanoparticles by sol-gel method while he characterized them using XRD, TEM, Mossbauer spectral and magnetic studies, where x ranged from 0 to 1.0. The sample particle size was approximately 6 nm on average which after annealing at a temperature of 1,000 ^{O}C increased up to 80 nm. The saturation magnetization decreased from 80.0 - 27.5 emu/g after annealing at 1,000^{O}C and increasing the Mg^{+2} ions because of the diamagnetic behavior of the Mg^{+2} ions [35].

Mukhtar Ahmad synthesized Single-phase "mono barium ferrites $Ba_{1-x}Sr_xFe_2O_4$ (x = 0.0, 0.33, 0.67, 1.00) by sol-gel auto-combustion method. A number of samples with x = 0.0 were heat treated at several different temperatures and then investigated by XRD analysis. An orthorhombic spinel like structure was discovered at 600°C, which is much lower than the temperature reported in some previous tests". Furthermore, the cell parameters such as V, a, b, c, Dx were altered subsequently by the Sr ions' substitution into the mono-barium ferrite although there was no change in the structure of these mono-ferrites was observed [36].

Erum Pervaiz observed low temperature sol–gel synthesis of Cr^{+3} and Al^{+3} substituted Co–Ni ferrites while x had a range of 0.0 - 0.25. He found that the X-ray density, lattice constant and Crystallite size decrease with increasing x concentration because it causes decrement in the atomic weights and ionic radii of the doping cations. Homogenously spherical and small particle sizes obtained due to sol–gel method at 90 °C. Because of an increment in Al^{+3} and Cr^{+3} concentrations to x=0.2, DC electrical resistivity of cobalt ferrite was enhanced to almost 108 (Ω-cm). Furthermore, the relaxation frequency and time for these ferrites were revealed with Electric modulus (Mn) and Complex impedance (Zn) analysis. This analysis also proved the grain boundary resistance's dominance for all the substituted cobalt ferrites [37].

A.I. Borhan studied the relations between magnetic, structural and electrical properties of zinc ferrites with Al^{+3} substitution. He synthesized $ZnFe_{2-x}Al_xO_4$ by sol–gel auto-combustion method with x from 0 to 2 tartaric acid as combustion complexion agent. He observed a slight decrease in the lattice constant and crystallite size with increase in aluminum content. The coercive and saturation magnetization field decreased nonlinearly with increase in aluminum content. It was also observed that the dielectric loss and dielectric constant decreases with increase in frequency but at high frequencies attains a constant value. [38].

T George observed "magnetic properties of cobalt ferrite nanoparticles synthesized by sol-gel method". The size of these particles had an average of 18 nm. The magnetization curves demonstrated a behavior towards the superparamagnetic range of the $CoFe_2O_4$ nanoparticles. Meanwhile, with an increase in the frequency, the microwave magnetic parameters showed a decreasing trend [39].

Mukesh C. Dimri prepared Barium monoferrite powders by citrate combustion technique. Heat treatment was done from 1100 to 1300 ^{O}C. Samples showed higher Curie temperature and larger coercivity compared to the values reported previously in literature. Dielectric constant ranged from 5-7 while permeability ranged from 2-6 both measured in

X-band frequency. Values of dielectric constant and permeability makes this material useful in microwave devices as well as a potential EMI shielding material [40].

M. T. FARID synthesized series of Gd-substituted Cobalt based ferrites of composition $CoGd_{2x}Fe_{2-2x}O_4$ for x= 0.00-0.25 via conventional ceramic technique. Dielectric constant values happened to be reduced with increasing Gd concentrations. AC conductivity showed semiconducting behavior over a wide range of frequency [41].

Md.D. Rahaman investigated structural, morphological and electromagnetic properties of $Mg_{0.25}Mn_{0.25}Zn_{0.5-x}Sr_xFe_2O_4$ ferrites synthesized via conventional solid state reaction method where x=0.00-0.20. XRD patterns showed single phase cubic spinel structures. Lattice parameters showed decreasing trend with increasing Sr^{+2} concentrations. The impedance spectra clearly revealed both grain and grain boundary effects on the electrical properties. Saturation magnetization showed a decreasing trend with Sr concentration. Due to decrease in saturation magnetization values, initial permeability decreased possibly due to dilution of tetrahedral-octahedral interaction with Sr^{+2} substitution [42].

A.A. Kadam synthesized $Ni_{0.8}Co_{0.2}Fe_{2-x}Dy_xO_4$ (x=0-0.1) ferrite samples by ceramic method. X-ray diffraction study confirmed formation of face centered cubic spinel structure. Dielectric constant and loss were observed to be reduced with increasing Dy concentrations. Impedance spectra portrayed grain contribution to conduction mechanism. Low coercivities showed the usefulness in magnetic shielding devices [43].

M. Kaiser studied Electrical conductivity and complex electric modulus of titanium doped nickel–zinc ferrites. Series of spinel ferrites $Ni_{1+x-y}Zn_yTi_xFe_{2\_2x}O_4$; y=0.1, 0.0-x-0.5 was synthesized. AC electrical conductivity showed a gradual change from semi conducting to semi metallic behavior as Ti^{+4} concentration increases. Electric modulus analysis showed mobility in low frequency regions assisted by hopping conduction while at higher frequencies mobility showed association with relaxation mechanism [44].

Naveen Kumari studied Structural, dielectric and magnetic investigations on Al^{+3} substituted Zn ferrospinels synthesized by chemical co-precipitation method. Dielectric properties decreased with increasing Al^{+3} concentrations. Saturation magnetization were decreased. coercivity and retentivity were found to be very small due to super-paramagnetic nature of particles [45].

Sagar E. Shirsath synthesized $NiFe_{2-x}In_xO_4$ (x = 0.0–0.30) samples through solid state reaction and investigated structural and magnetic properties. Curie temperature traced from susceptibility plots showed decreasing trend with indium substitution. The decrease in Curie temperature is attributed to weakening in A–B interactions [46].

A.P. Singh etaal. Studied the microwave properties of conducting magnetic nano composites. They suggested that the electromagnetic properties of a composite having multiple phases can be improved by various methods. These methods include introduction of magnetic filler in a reasonable amount. Other method involves the design of such a medium that contain conducting magnetic and dielectric material mixture as filler. A lot of studies have done in this field, but scientists are still unable to find out a material that will produce no reflection and give competent absorption. This is a challenging task the only possible solution is the use of materials which can also be seen as the future possibility. The next generation material will form the building blocks of shielding material will be multi-phase and lightweight materials having excellent shielding properties [47].

H.S. Singh et al. worked on ferrite nanoparticles due to their remarkable dielectric and electric properties. They worked on nickel ferrite and substituted nickel ferrite. The magnetic, electric and physical properties of nickel showed a remarkable improve when it is substituted with Aluminum. So, it can be concluded that the properties can be enhanced by making composite of nickel with other material. The study is needed to know the exact amount of substitution and method of preparation. The effect of preparation technique should also be known [48].

2.3 Preparation of $Ba_{1-x}Co_xFe_2O_4$

For the synthesis of $Ba_{1-x}Co_xFe_2O_4$ with x= 0.00 ,0.20 ,0.35 ,0.50 ,0.75, 1.00 we used sol-gel auto combustion method.

2.3.1 Apparatus

- Beaker
- Magnetic stirrer
- Heating plate
- Permanent magnet
- Spatula
- Mortar and pestle
- China dishes

2.3.2 Chemicals

- Barium nitrate [$Ba(NO_3)_2$]
- Citric acid [$C_6H_8O_7$]
- Ammonia solution [NH_4OH]
- Cobalt nitrate [$Co(NO_3)_2 . 6H_2O$]
- De ionized water
- Iron nitrate [$Fe(NO_3)_2 . 9H_2O$]

All the above-mentioned materials were analytical grade and was provided by ACROS organics, Sigma Aldrich and EMSURE®.

2.3.3 Procedure

For synthesis citric acid and metal nitrates ratio was kept as 3:1 and following stoichiometric ratio formula was used to calculate the composition of different chemicals utilized in the process.

$$Mass(g) = \frac{\text{Molarity } \times \text{Molecular mass} \times 100}{1000}$$

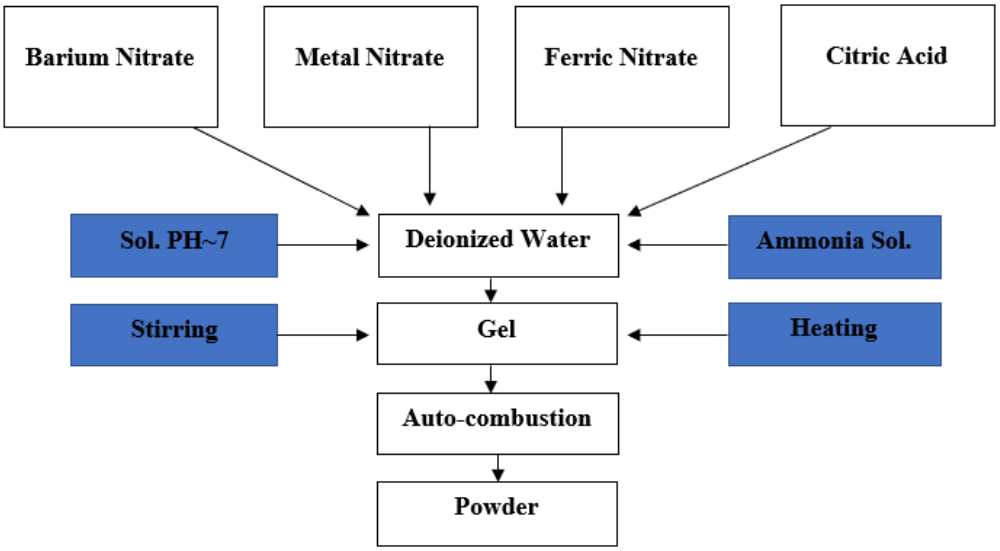

Figure 7. Flow Chart Diagram for the Synthesis of $Ba_{1-x}Co_xFe_2O_4$

Barium nitrates, iron nitrate and citric acid (3M) were dissolved in stoichiometric amount in 100ml of deionized water. Each solution was magnetically stirred for at least 15 minutes until they form a clear solution. Then after combining all the solutions together ammonia solution was dropwise added until pH changed to 7. We, then heated the mixed solution at 300°C with continuous stirring. The solution formed a dark brown color and became a viscous gel because of continuous evaporation. The gel ignited and burnt after we removed all the water particles, until the whole citric acid was consumed. After the completion of combustion dark brown color ashes were formed. Ashes were then collected using spatula and grinded using mortar and pastel and then sintered at 800 °C in muffle furnace for 4 hrs. For doped samples cobalt nitrate along with barium nitrate, iron nitrate and citric acid was dissolved in their stochiometric values and whole process explained above was repeated.

2.4 Sample Preparation for Testing

For FTIR, Electric and magnetic properties sample were prepared using different techniques given below

2.4.1 Sample Preparation for FTIR

KBr pellet method was for sample preparation because alkali salts give no absorption in IR spectrum. Small amount of sample and KBr was taken and ground to fine powder and pellet was prepared using pellet die set and hydraulic press. Mixture of ground KBr and sample was added into the die and it was then placed in hydraulic press system at 3 tones for almost 15 seconds, and then was released and die was taken out. Finally, a thin sample pellet having thickness in the range of 2-3 mm and dia of ~13 mm was obtained. We heated the samples at 100 ℃ for almost 20 minutes for the removal of moisture.

2.4.2 Sample Preparation for Dielectric Measurements

For measurement of electrical properties of samples, pellet of each sample was prepared using pellet die set and Hydraulic press. Each sample was finely grinded before sample preparation. Pellets were prepared using ~ 0.8 gram of each sample using hydraulic press at a load of 4 tonnes for 2 minutes on each pellet. Thickness and diameter of prepared samples was measured by vernier caliper. The prepared pellets were kept at 700 ℃ to be sintered for 2 hrs and used for measuring dielectric behavior. Figure 2.3 shows prepared samples for Dielectric analysis.

Figure 8. Prepared Samples for Dielectric Properties Analysis

2.4.3 Preparation of Samples for the Measurement of Magnetic Properties

For magnetic analysis via VSM, pellet of each sample was prepared using small die of almost 2mm dia. Finely grounded samples of ~ 0.3g were placed inside the die, which was then placed inside hydraulic press at ~2 tonn pressure for 2 minutes. After removal of pressure, samples were removed from the die and then used for Magnetic analysis.

Chapter 3

Sample Characterization Techniques

The properties of $Ba_{1-x}Co_xFe_2O_4$ are analyzed by performing different analysis techniques. Information about physical and chemical behavior of material along with surface morphology, lattice parameters etc. can be obtained. This chapter will shortly cover the characterization techniques. Following techniques can be used for the analysis of synthesized ferrites.

3.1 X-Ray Diffraction Technique

It is a useful tool for the identification of degree of crystallinity and structure of a material. Clear information about structural strain, crystal defects, average crystallite size, crystallographic orientation and degree of crystallinity can be obtained by using XRD. Three different methods can be used for finding out crystal structure i.e. powder diffraction method, Laue method and rotating crystal method. Two techniques can be used to determine crystal size if powder diffraction method is used. Those techniques are as follows.

- Debye Scherrer Method
- Diffractometer method

In present research, samples were analyzed with CuK_α from X – Ray Diffractometer system. The X rays had a wavelength of 1.5405 Å and the analysis was made at room temperature. The scanning rate was relatively low at ~2^o/min at 20mA and 40kV with a resolution of 0.011, while the scanning range was 20^o to 80^o. These patterns were then analyzed with “Stoe-Seifert X’PERT PRO-Highscore” while Cu-alpha=1.54 source was the XRD.

3.1.1 Basic Principle of XRD

The powdered sample is placed for analysis. X-ray beam is made to fall on the sample and reflected from plane of crystal. The crystal plane reflects the X-rays that are incident on material. Then interference only takes place when incidence angle is exactly same as reflection angle. The Bragg's Law is given by

$$\mathbf{2d\ Sin\theta = n\lambda} \quad \text{.....(3.1)}$$

n is order of interference, θ is incidence angle, d is Interlayer distance and λ is incident X-ray wavelength. Figure 3.1 shows atomic plane arrangement in a crystal structure.

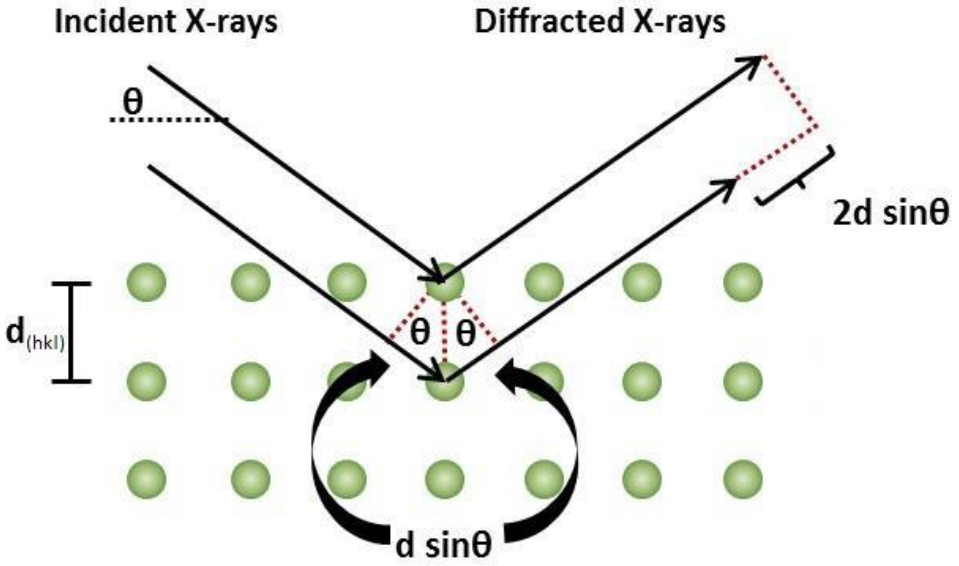

Figure 9. Incident X-ray Beam Scattered by Atomic Plane in a Crystal [42]

The Bragg's law states that the incident ray is reflected only when the path difference between set of planes is 2dsinθ [49]. The set of planes are at an equal distance of d. Following is the condition required for constructive interference:

$$\mathbf{2\ d\ sin\ \theta = n\ \lambda,}\ \text{where } n = 1,2,3$$

The condition for reflection in above mentioned equation is that it only occur when θ<2d. For this reason, visible light cannot be used. For the characterization of a three dimensional structure three techniques are usually used which are as follows:

- Laue method
- Powder method
- Rotating crystal method

The sample which is to be characterized using XRD is in the form of Nano powder. So, the powder method will be the one useful for the desired sample. For the evaluation of powdered sample and in the case of in availability of single crystal of acceptable size, powder diffraction is the best method to be employed. The procedure of this experiment includes the crushing of sample into fine powder. Afterwards the sample will be placed in aluminum or glass rectangular shaped plate. A monochromatic X-ray beam is then directed towards the powdered sample.

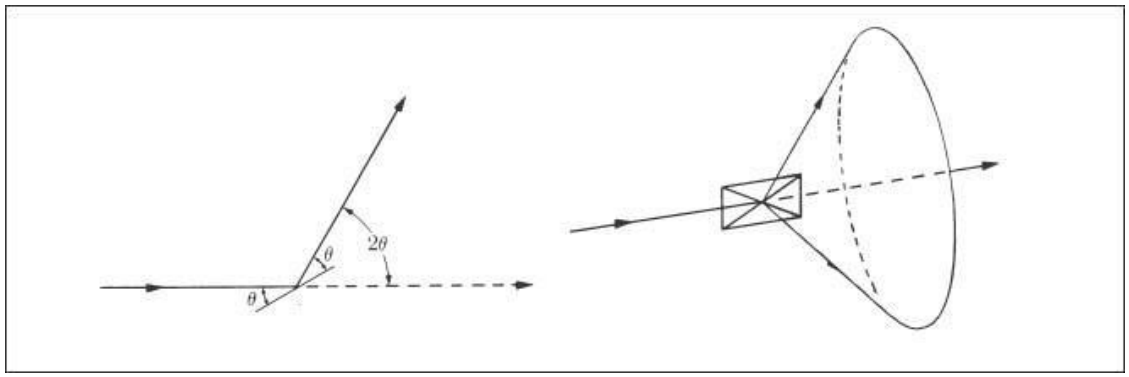

Figure 10. Diffracted Cones of Radiations Forming in Powder Method [42]

Consider the reflection as shown in figure 10. The fraction of sample, which is in powder form, is at such an orientation which will enable reflection by being present at correct Bragg angles. When the plane is rotated about the beam which is made incident, the path of motion of reflected beam will be across the surface of cone. In the case of our particles the reflection does not occur across the surface, a large number of crystal particles will have same reflections and some of those reflections will be able to satisfy brags law. The inter planner spacing, d, can be calculated using λ and θ.

Lattice Constant

Lattice constant defines the unit cell of a crystal and is usually defined as the length of one edge of the cell or an angle forming between edges. It can also be termed as lattice constant or lattice parameter. The distance, which is constant, between the lattice points is known as lattice constant. Following equation is used to calculate lattice constant.

$$a = \frac{\lambda(h^2+k^2+l^2)}{2Sin\theta} \text{ ……..(3.2)}$$

In the above equation, lattice constant is "a", the wavelength of X - ray radiation is 1.54 A° for Cukα, miller indices are "h, k, l" and diffraction angle is θ radian or degree.

Crystallite Size

For the identification and confirmation of the experimentally obtained diffraction pattern it is compared to JCPDS cards. The structural properties are greatly influenced by particle size. According to Debye Scherrer equation, which is used to calculate particle size, crystal size is inversely proportional to peak width. So, the small crystallite size is related to peak broadening in XRD analysis. The Debye Scherrer equation is used to calculate particle size.

$$t = \frac{0.9\,\lambda}{\beta Cos\theta} \text{ ……(3.3)}$$

λ represents the incident X-ray wavelength and θ and β represent diffraction angle and full width half maximum respectively.

3.2 Fourier Transform Infrared Spectroscopy

The absorption, emission spectra, ramman scattering, and photoconductivity of the material can be obtained by using this analytical technique. The stretching modes of the elements present in composite and chemical purity of a material is determined using FTIR. It collects the data from spectrum of matter. FTIR is used to determine the amount of light that a sample absorbs at a specific wavelength.

3.2.1 Working of FTIR

In FTIR, a polychromatic source produces an infrared light which falls on the splitters. One half of this incident light refracts into the direction of the fixed mirror while the other half transmits through the moving mirror. This second half goes through the sample. The information about molecular component and structure of the sample can be obtained by interaction of light with sample

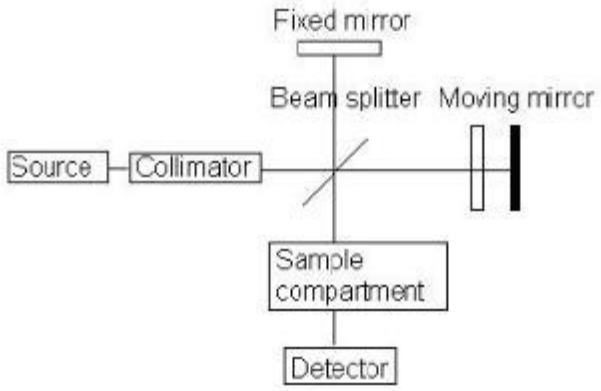

Figure 11. Schematic Figure of Fourier Transform Spectroscopy [46]

It is a sensitive technique and can also be used for identification of many organic compounds for example, paints, polymers, resins, coatings and drugs etc. it is the only analytical technique which provides ambient temperature operation and capability of monitoring the vibrations of functional groups directly, which are used for characterizing molecular structure and governing the course of chemical reactions [50] . IR radiations lie between the microwave and visible light and has a wavelength smaller than the microwaves and longer than the visible rays. The frequency of IR radiations is higher than the microwaves but is lower than the visible waves. IR region can be sub-divided to three regions: the near, mid and far IR regions. Near IR region is the portion closer to the visible region of spectrum, while far IR region is the portion of waves closer to the microwave region, and the mid IR region, as the name suggests, is between these two regions. Thermal radiations are considered as a primary source of IR radiations. IR radiations are produces

because of the motion of atoms and molecules in the sample. Higher temperatures cause more vibration and thus more IR radiations.

According to the principle of FTIR, when the applied IR frequency matches the natural frequency of vibration, molecular vibrations are produced. Different frequencies are required by every different bond or functional groups for these vibrations. [51].

3.2.2 Applications of FTIR

The components of a mixture are separated using gas chromatography

- The analysis of liquid chromatography fraction can be done using FTIR.
- Tiny samples can be checked with the help of infrared microscope in sample chamber.
- The sample having emitted spectrum of light is obtained FTIR in place of light spectrum through the sample [52].

3.3 Electrical Properties

Dielectric properties are measured using impedance analyzer pellet is placed in pellet holder and connected to device.

3.3.1 Dielectric Properties

Dielectric properties such as conductivity, dielectric loss and dielectric constant were determined using the E4991A RF Impedance and material in frequency ranges from 1MHz to 1GHz. Tan loss, dielectric loss ε'' and Dielectric constant ε' are directly determined from the data. The permittivity has imaginary and real components such that

$$\varepsilon = \varepsilon' - j\,\varepsilon'' \quad \text{.....(3.4)}$$

Also the formula used to calculate AC conductivity is:

$$\sigma_{a\,c} = \omega\,\varepsilon\,\varepsilon_o\,\tan\delta \quad \text{.....(3.5)}$$

While the equations below were used to calculate the real and imaginary part of the complex electric modulus.

$$\mathbf{M'} = \frac{\varepsilon'}{\varepsilon'^2+\varepsilon''^2} \text{ .....(3.6)}$$

$$\mathbf{M''} = \frac{\varepsilon''}{\varepsilon'^2+\varepsilon''^2} \text{ .....(3.7)}$$

3.3.2 Electronic and Atomic polarization

When the dielectric material is placed within the electric field the electron cloud of atoms is displaced relative to nuclei in atom, which produce an induced dipole moment in the molecule.

3.3.3 Ionic Polarization

Ionic polarization take place in solids with ionic bonding having dipoles, but these dipoles get cancel due to the symmetry of the crystals structure. In the presence of applied electric field positive and negative ions are displaced from their equilibrium positions hence inducing dipole moment.

3.3.4 Dipolar and Orientation Polarization

It is only applicable to the polar dielectric materials. In the absence of electric field dipoles are randomly oriented so the sum of their dipole moment is zero. When these polar dielectric materials are placed within the electric field these dipoles rotate and align themselves in the direction of electric field.

3.3.5 Interface and Space charge Polarization

Space charge polarization take place due to the diffusion of ions along with applied electric filed. It usually occurs due to the accumulation of charges in the interface or at the grain boundaries of the material.

3.3.2 AC Impedance Spectroscopy

We measured the AC impedance parameter at room temperature, Resistance (R) and reactance (X) were measured over the frequency range of range of 1MHz to 1GHz. The impedance is a complex quantity where resistance (R) and reactance (X) shows the imaginary and real parts of impedance in the circuit by the relation.

$$\mathbf{Z=R+j\,X} \text{ ……...(3.8)}$$

The impedance Cole-Cole plot shows the resistive behavior of the material. The SI unit of impedance is 'Ω' where resistance (R) and reactance (X) shows the imaginary and the real parts of impedance in the circuit by the relation.

$$\boldsymbol{R = Z' = |Z|cos\theta} \text{ ……...(3.9)}$$

$$\boldsymbol{X = Z'' = |Z|sin\theta} \text{……....(3.10)}$$

CHAPTER 4

Result and Discussion

4.1 XRD Analysis

After calcination we obtained the X-Ray diffractograms of the synthesized samples of the form $Ba_{1-x}Co_xFe_2O_4$ with x= 0.00 ,0.20 ,0.35 ,0.50 ,0.75 , 1.00 at room temperature. Sample with x=0.00 showed polycrystalline pattern which could be indexed to the reflection planes of (212), (610), (020), (004), (422), (614) and (630), which proves the distinct orthorhombic structure formation as shown in Figure.12. The diffractograms for x = 0 resembles the reference data of JCPD No.00-025-1191 with Pnma-E space group.

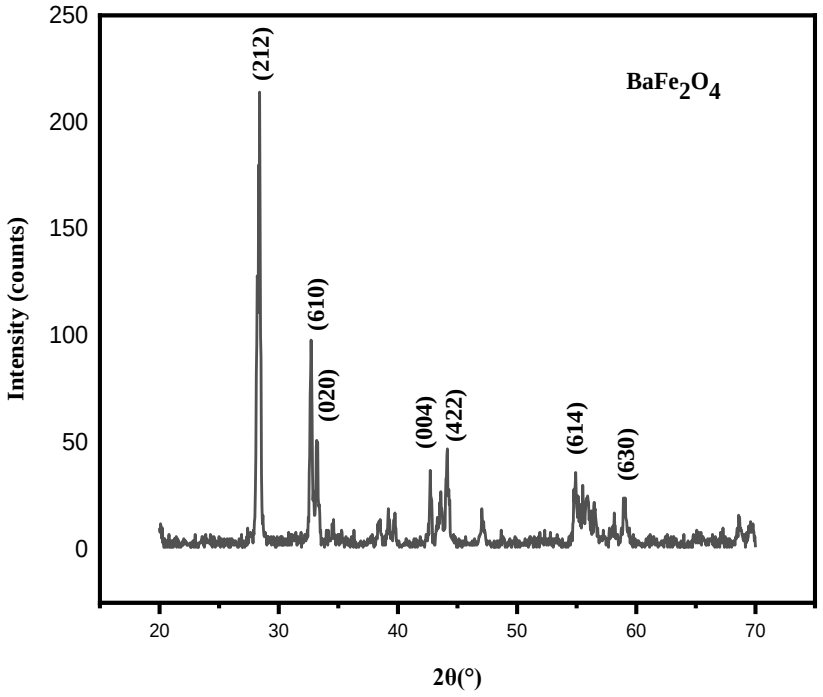

Figure 12. XRD Spectra for $BaFe_2O_4$

Same pattern is observed in testing the remaining compositions of x, which indicates that there is no additional peak confirming that the samples are pure. As evident from the graph a decrease was observed in the intensity of diffraction peaks and a shift in diffraction peaks is observed for $x \geq 0.5$ indicates structural changes from orthorhombic to cubic system. Since the intensities of reflection plane (220) and (440) were sensitive to the cationic distribution at B and A, they were affected the most. The increase in the relative intensities of these planes shows the preferential occupancy of Cobalt ion by both Tetrahedral and Octahedral sites. But if relative intensities are compared, the increase in intensity of plane 220 is comparatively lower than that in the plane 440. This behavior shows preferential occupation of the substituted cobalt ions on B site and a minute tetrahedral A site occupancy [53] [54] [55]. At x=1.00 pure cubic structure with peaks (220),(313),(222),(400),(422),(511) and (440) has been formed with reference data of JCPD No.00-022-1086 as shown in Figure.13.

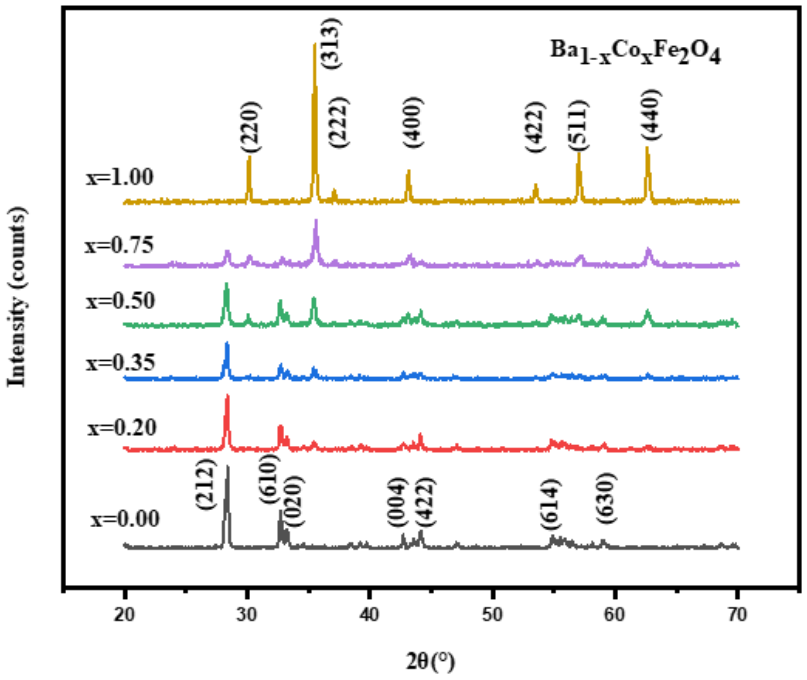

Figure 13. Indexed XRD Spectra for $Ba_{(1-x)}Co_xFe_2O_4$

We observed the crystallite size and calculated this size to be in nanoscale from a range of 26nm to 40nm.

4.2 FT-IR Analysis

The FT-IR spectra verify the single phase formation of ferrites by facilitating the analysis of ions positioning throughout the crystal lattice through their vibration modes. The lattice parameters, distribution of cations, masses of cations and associated force constants have a significant effect at the vibrational frequencies of oxygen ions with cations. The infrared spectral measurements of Co^{+2} substituted $BaFe_2O_4$ were carried out at room temperature in the wave number range of 350-1000 cm^{-1} and are shown in Figure.14. As reported by Waldron [56], each spectrum exhibits two strong absorption bands $\boldsymbol{v_1}$ and $\boldsymbol{v_2}$,which correspond to stretching vibrations of tetrahedral $\boldsymbol{v_1}$ (A-O-A) and octahedral $\boldsymbol{v_2}$ (B-O-B) metal oxygen complexes respectively. The observed spectrum for each composition confirmed the formation of single phase spinel structure of ferrite with $\boldsymbol{v_1}$ in the range of 566.41-623.42 cm^{-1} and $\boldsymbol{v_2}$ in the range of 383.11-499.89 cm^{-1}. The absorption peak at 772 cm^{-1} for samples x=0.00.0.20,0.35 represented the vibration of Ba–O [57]. Owing to different bond lengths of Fe-O at octahedral and tetrahedral sites, frequency bands at which $\boldsymbol{v_1}$ and $\boldsymbol{v_2}$ appear show difference. The decrease of lattice parameter also shrinks the dimensions of the unit cell, which in turn affects the Fe-O positioning. Co^{+2} has smaller ionic radii than Ba^{+2} but larger than Fe^{+3}. Co^{+2} can occupy both A and B sites. Depending upon placement of Co^{+2} on tetra and octahedral sites, the relative bond lengths increases or decreases in respective sites thus changing octa and tetrahedral band frequencies.

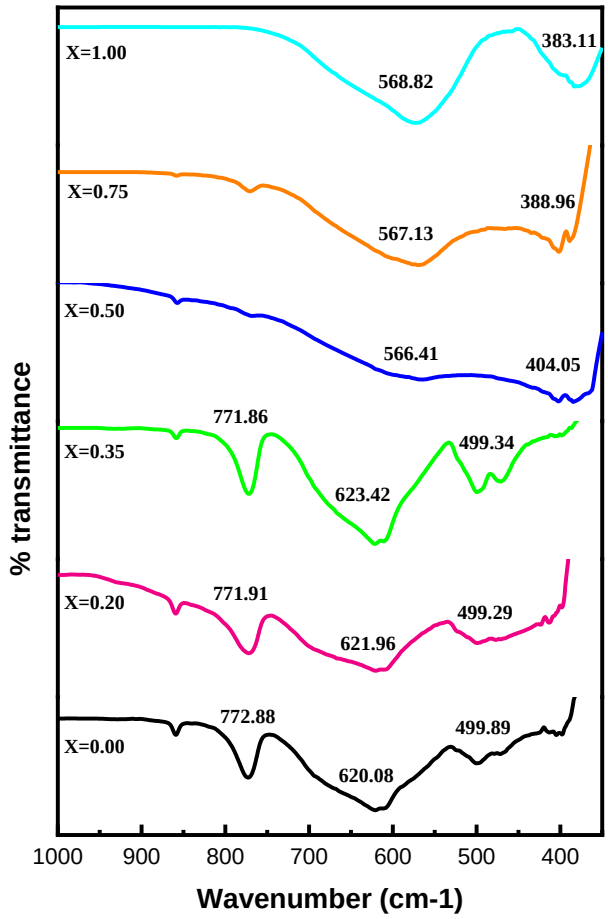

Figure 14. FTIR Spectra of $Ba_{(1-x)}Co_xFe_2O_4$

From figure.14, a relatively wide range of ν_1 is observed for x=0.00-0.35. this wide range suggests that variation of the lattice parameter with Co substitution is dominated by the variation of the tetrahedral sublattice radius [58] while for further higher concentrations, variations in ν_2 is observed which suggests dominance by variation at octahedral sites.

4.3 Dielectric Results

The dependence of impedance, dielectric loss, tan loss, AC conductivity, modulus and dielectric constant on frequency is calculated through sintered pallets using standard calculations.

4.3.1 Dielectric Constant:

Permittivity of a material is defined by its ability to polarize in presence of electric field. The dielectric parameters were calculated by "RF Impedance analyzer" with a frequency range of 1MHz to 1GHz. Pallets (sample) were prepared with average 13mm dia and 2mm thickness. Dielectric permittivity is defined as $\varepsilon r = \varepsilon' + i\varepsilon''$ Where εr represents dielectric permittivity of a medium, ε″ and ε′ are the imaginary and real parts of it. The electromagnetic energy storage is attribute of real part while imaginary part attributes for thermal conversion also known as dielectric loss. The dielectric properties of $Ba_{(1-x)}Co_xFe_2O_4$ where (x = 0.0, 0.20, 0.35, 0.50, 0.75, 1.00) are calculated and the effect of increasing frequency has been studied.

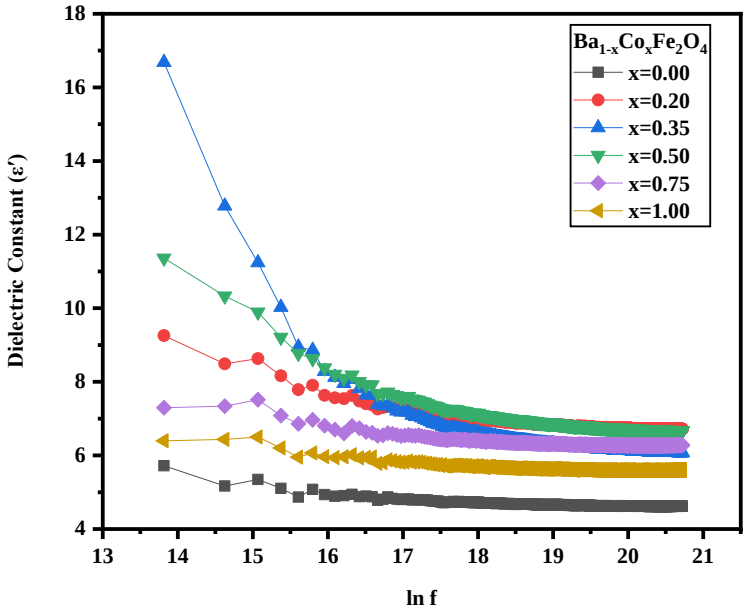

Figure 15. Dielectric Constant's Variation with Frequency

Figure.15 shows effect of frequency on dielectric constant. A decreasing trend of dielectric constant with respect to frequency is observed. It is a normal dielectric dispersion which can be narrated by the Maxell- Wagner type interfacial polarization [59]. In any material interfacial, ionic, electronic and dipolar polarizations contributes to the dielectric constant. Dipolar and interfacial polarizations are significant at low frequencies while at high frequencies electronic polarization paly more vital role towards dielectric constant [60]. When we apply the field, the electron initially piled up at the grain boundaries causing polarization. However, as the frequency increase the electron exchange from Fe^{+2} to Fe^{+3} slows down as the time required to change the direction with the field is not met which produces a decrease in polarization and thus a decrease in dielectric constant [38]. The dielectric constant increases till x=0.35 then a decreasing trend is observed. This irregular trend of dielectric constant is because of the cation deposition. For the lower concentrations, till x=0.35, Co^{+2} ions reside at tetrahedral sites and hopping of Fe^{+2}/Fe^{+3} ions increases. At higher concentrations Co^{+2} ions start replacing Fe^{+3} ions on octahedral sites, moving Fe^{+3} ions to tetrahedral sites reducing the concentration of Fe^{+3} ions on octahedral sites which play an important role in the dielectric polarization. These movements of ions reduce the hopping mechanism , hence decreasing the dielectric constant [61].

4.3.2 Dielectric Loss:

Figure.16 presents the behavior of dielectric loss with respect to frequency. The dielectric loss is found to have higher values at lower frequencies, but it decreases at higher frequencies because of decrease in polarization. This behavior is observed because of the conduction mechanism in ferrites. This mechanism is explained by Koop's phenomenological model [9]. This model states that at low frequencies grain boundaries are more dominant. So, at low frequencies, resistivity is higher hence loss is higher in low frequency region resulting in large amount of energy requirement for exchange between Fe^{+2} and Fe^{+3} ions. At high frequencies resistance offered by grain boundaries reduces hence dielectric loss reduces to a constant value [9].

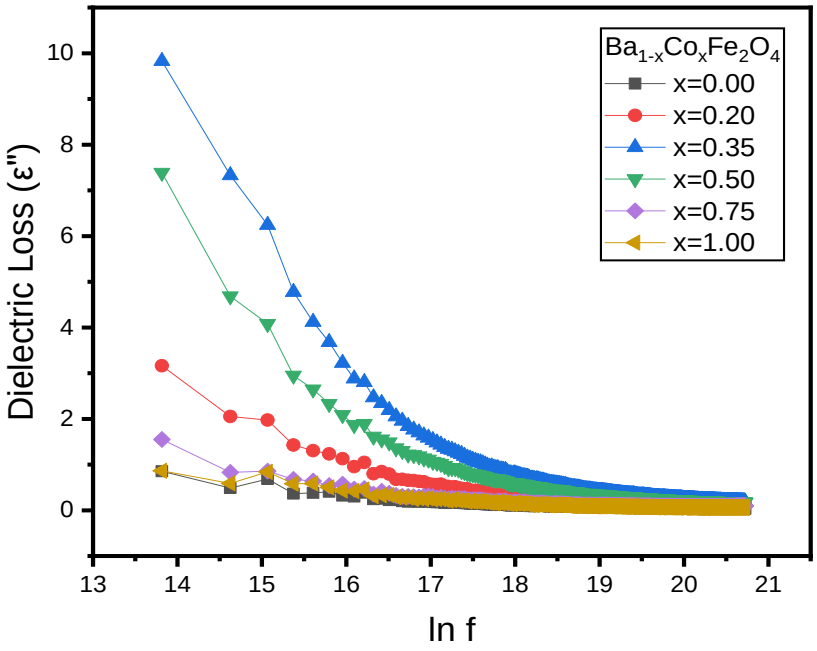

Figure 16. Dielectric Loss Behavior with Frequency

4.3.3 Tan Loss:

Tan loss quantifies the relative energy loss across a large frequency range due to varying electric field. Dielectric tangent loss is caused by the lag in polarization with increase of applied electric field. Figure.17 shows compositional changes in tan loss with increase in frequency. We observed that with increase in the concentration of cobalt, dielectric tangent loss values have been increased. The reason could be variation in grain size, impurities or imperfections in the crystal lattice.

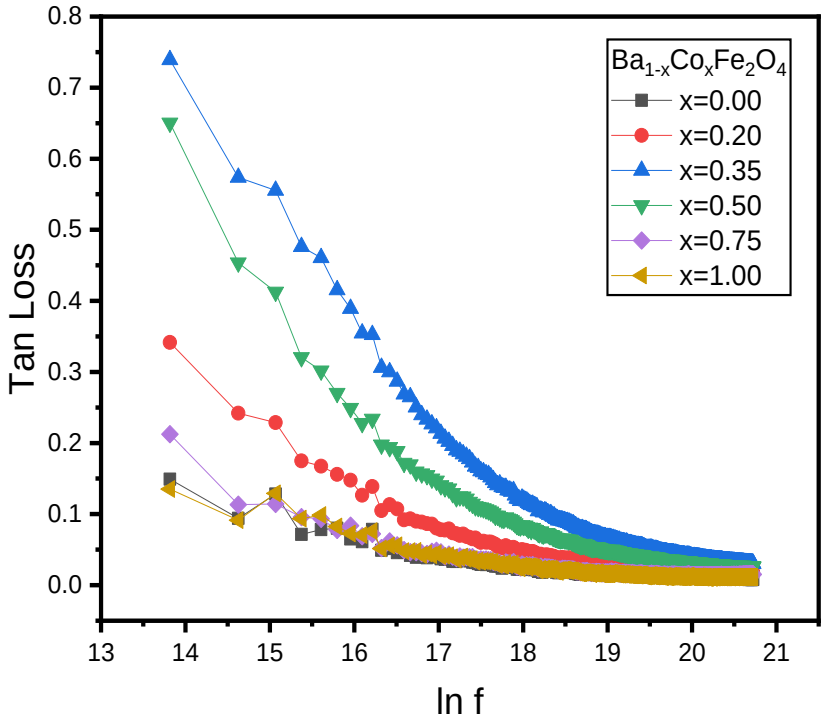

Figure 17. Tan Loss Behavior with Frequency

Tan loss values are observed to be higher at lower frequencies and they decrease with increasing frequencies. Figure.17 shows normal tan loss trend, we observe a higher loss at lower frequencies due to greater energy losses by highly resistive grain boundaries, these grain boundaries are less resistive in high frequency regions so tan loss value reduces significantly at higher regions [9] .

4.3.4 AC Conductivity:

Conductivity of a material is its quantification of how conductive or resistive a material is. In ferrites, the process of conductivity is precisely because of the electrons jumping from ions of the same element with different valence state. In our research, we calculated the conductivity of all the samples using:

$$\sigma ac = 2\pi f \varepsilon o \varepsilon''$$

f represented the frequency, ε_o represents the permittivity of free space and ε'' represents dielectric loss. The trend of AC conductivity is presented in figure.18. At lower frequencies conductivity is almost independent of frequency and significantly increases with increase in frequency. The stated behavior can be explained using Maxwell-Wagner type interfacial polarization [59]. Conductivity is low at lower frequencies due to large hindrance offered by grain boundaries. With increasing frequency, conduction across grain boundaries increases because of more jumping electrons between Fe^{+2} andFe^{+3} ions [62]

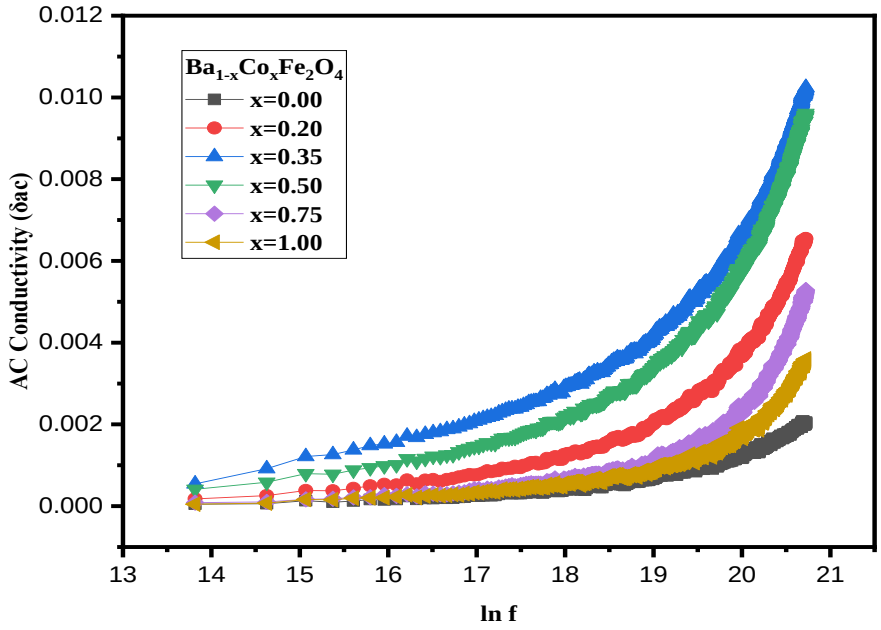

Figure 18. AC Conductivity with Frequency

4.3.5 Complex Electrical Modulus (Real Part)

Electric modulus formalism is a crucial tool for characterization of conduction and relaxation behavior for ionic and electronic conducting materials. Figure.19 shows real part of electric modulus. The observed values of M' for all the samples under consideration are less in low frequency range representing negligible electrode effect [63]. A continuous increase in modulus is observed with frequency. The magnitudes in M' tend to saturate at

higher frequencies that may have originated from the short-range mobility of charge carriers [63].

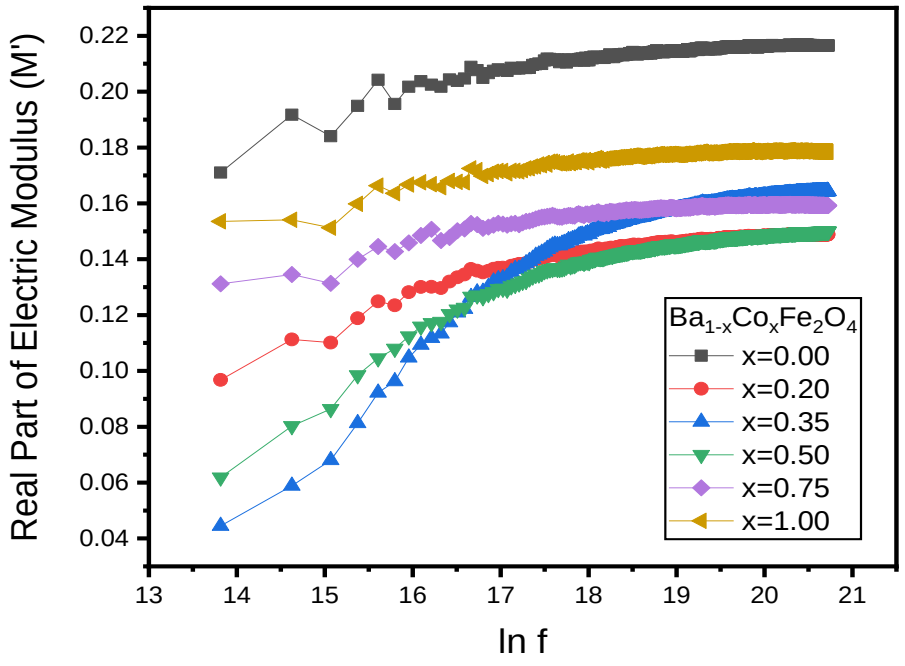

Figure 19. Real Part of Electric Modulus with Frequency

4.3.6 Imaginary Part of Electric Modulus

Figure.20 presents the change in imaginary part of electric modulus with changing frequencies.

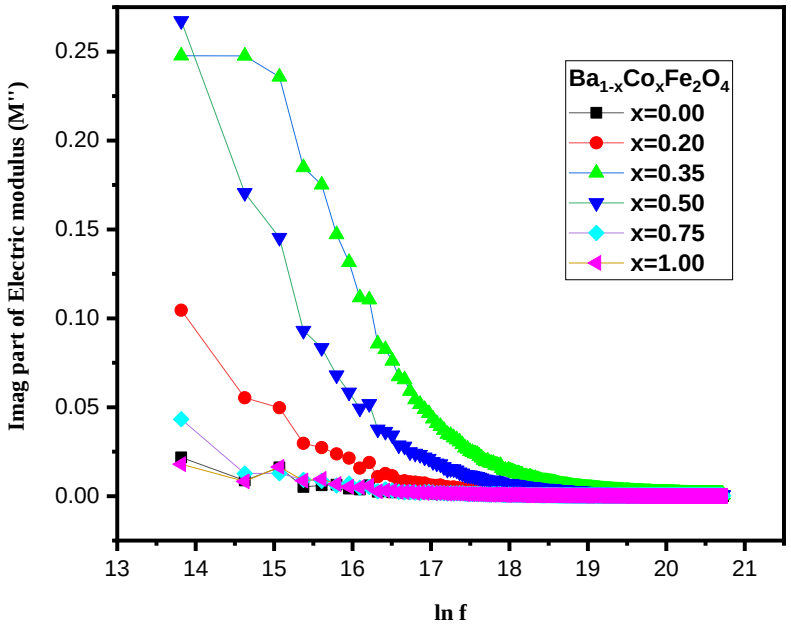

Figure 20. Imaginary Part of Electric Modulus with Frequency

It is obvious that the dielectric response for x=0.35 is well resolved by semicircle arc showing relaxation peak (maxima) and hence the relaxation mechanism can be explained easily. Modulus (M″) might have increased with the increase in the applied oscillating field(which is beyond the frequency range of my study) and reaches a highest value at some frequency (relaxation frequency), where the oscillating dipoles frequency and applied frequency coincides and then decreases further. But for other concentrations, the maximum frequency of M"(f) is shifting towards lower frequency regions that shows grain boundary contribution to resistance is greater for other compositions [64] . The decrease in relaxation frequencies show increase in relaxation rate as peaks are shifting towards lower frequency region.

4.3.7 Cole-Cole Plots

The complex modulus plots, also known as cole-cole plot is shown in figure.21. It is obvious that cole-cole plots for compositions x=0.75 and 1.00 have poorly resolved semicircle arcs with maxima somewhat in lower frequency regions. This behavior of

modulus shows that relaxation phenomenon is absent for higher concentrations and the loss associated with this relaxation is also minimized [64].

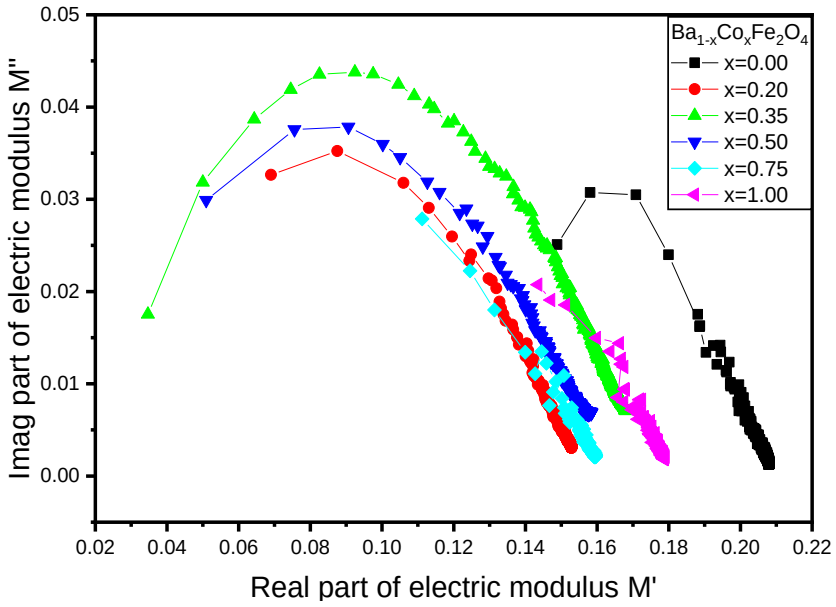

Figure 21. Complex Modulus Plane Plot (M" vs. M')

Figure.22 shows cole-cole plot of impedance of all samples. Cole-Cole plot analysis we can differentiate the resistance effect of intrinsic grain, grain boundaries, sample-electrode effect, defects, and relaxation process etc. Appearance of semicircles represent a relaxation process and radius of semicircle represents resistance of sample whose center lies on Z' axis if the conduction is Debye type.

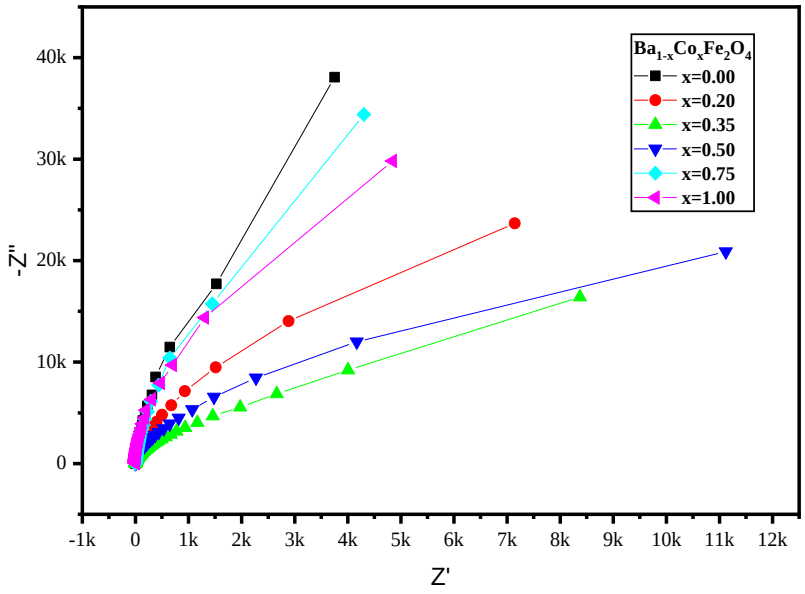

Figure 22. Complex Impedance Spectra

The decrease in radius of semicircle with increasing dopant concentrations show decrease in resistance of samples. For x=0.35, minimum resistance of sample is observed.

4.4 Magnetic Properties

There is a big number of factors that affect the magnetic characteristics of a material including intrinsic factors such as particle size, crystal defects and lattice strains, and also by some extrinsic factors like powder density, microstructure, chemical composition and synthesis route [65] [66]. Figure.23 shows magnetic behavior of $Ba_{(1-x)}\,Co_x\,Fe_2\,O_4$, x = 0.00, 0.02, 0.35, 0.50, 0.75, 1.00. Magnetic parameters such as saturation magnetization (Ms), remanent magnetization (Mr), isotropic property (Mr/Ms), and coercivity (Hc) were measured at room temperature and a vibrating frequency of 40 Hz. The values of these parameters were extracted from the loops and are shown in Table 1. Variations in these parameters can be justified with various explanations. Table 1 indicates a linear increase in remanence and saturation magnetization, which can be directly related to the increase in net magnetic moment. The result indicates that saturation magnetization increases as the concentration of cobalt increases. This behavior can be explained on the basis of individual magnetic moments of Co^{+2} and Ba^{+2} ions. Ba^{+2} ions have no magnetic moment due to all paired electrons while Co^{+2} has a magnetic moment of 3.87BM. By replacing cobalt with barium, the effective magnetic moment increases [67] [68]. Increase in cobalt concentration increases the availability of ions with greater magnetic moments hence increasing the overall magnetization of sample. Cobalt ions replace barium ions on tetrahedral sites as the dopant concentration increases. An increase in number of magnetic ions on A sites increases the A-B interactions thereby increasing curie temperature [69]. Increase in remnant magnetization may be attributed to the increase in exchange interactions with increasing cobalt concentrations [35].

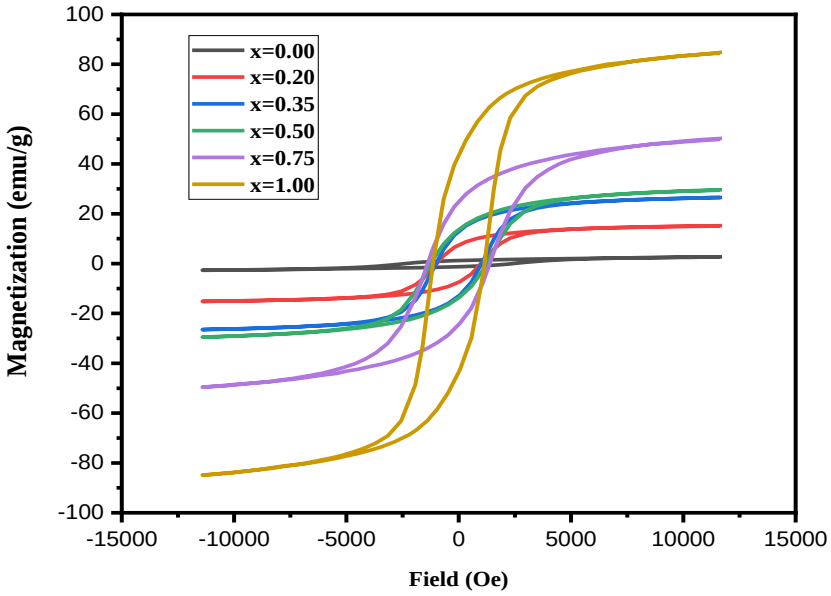

.Figure 23. Room Temperature M-H Curves for $Ba_{(1-x)}Co_xFe_2O_4$

Table 1. shows the data collected through magnetic analysis. Saturation magnetization and remanence shows an increase with increasing concentration of cobalt.

Table 1. Magnetic Parameters of prepared samples.

X	M_s(emu/g)	M_r(emu/g)	H_c(Oe)	M_r/M_s
0.00	2.69	1.23	2402	0.459
0.20	15.2	7.40	981	0.487
0.35	26.5	8.88	1009	0.487
0.50	27.7	13.6	1235	0.490
0.75	49.9	24.2	1378	0.492
1.00	84.8	43.1	1141	0.512

Conclusion

Cobalt doped barium mono ferrite nanoparticles have been synthesized successfully by sol-gel auto combustion method showing pure orthorhombic structure which shifts to cubic crystal structure with increasing cobalt concentrations which was confirmed by XRD analysis. Tetrahedral and octahedral frequencies were analyzed through FTIR analysis which showed shifts in vibrational frequencies by increasing dopant concentrations. Electrical and magnetic properties have been investigated for the use of cobalt doped barium monoferrite in high frequency devices. Frequency dependent dielectric behavior has been studied in the frequency range (1MHz-1GHz). All samples showed dielectric dispersion and polarization phenomenon. Dielectric constant increased to a highest value of 16.7 with concentration x=0.35. Further decrease of dielectric constant has been observed possibly due to the placement of cobalt ions at different sites which lead to decrease in hopping mechanism. Dielectric losses and tan losses showed similar behavior. AC conductivity increases linearly with rising frequency and reaches to a maximum value of x=0.35 and a further decrease in AC conductivity is observed with increasing cobalt concentration. Electric modulus affirms the absence of relaxation phenomenon at high frequencies. Electric impedance showed resistance of samples by appearance of semicircles having centers lied along Z' axis with minimum resistance for x=0.35 concentration. Magnetization of samples increased with increasing cobalt concentrations.

Future work

Electrical and magnetic properties of $Ba_{(1-x)}Co_xFe_2O_4$ can be further studied with varying concentrations or by co-doping with other metals. Composites with different polymers can be produced to study electric, magnetic and optical properties. Optical properties of $Ba_{(1-x)}Co_xFe_2O_4$ can be studied by UV-Visible spectroscopy which can be helpful in military applications. Microwave properties of prepared sample can be studied for microwave absorption devices and wastewater applications.

References

[1] S. &. S. H. Amiri, J. Materials Science and Engineering 33 (2013) 1-8.

[2] A. K. S. R. K. &. S. Yadav, J. Sensors and Actuators B: Chemical 229 (2016) 25-30.

[3] M. Sugimoto, J. Journal of the American Ceramic Society 82 (1999) 269-280.

[4] M. &. H. A. Wu, J. Academic Press (2013).

[5] K. S. K. B. S. &. M. S. R. Praveena, J. Journal of Magnetism and Magnetic Materials 321 (2009) 2433-2437.

[6] R. W. N. J. S. W. &. S. L. A. Babbitt, J. U.S. Patent and Trademark Office (1970).

[7] S. &. T. J. Bierlich, J. IEEE transactions on magnetics 48(4) (2012) 1556-1559.

[8] F. G. Brockman, J. Electrical Engineering 68 (1949) 1077-1080.

[9] D. S. &. J. R. S. Mathew, J. Chemical engineering journal 129 (2007) 51-65.

[10] C. W. Chen, "Magnetism and metallurgy of soft magnetic materials," Courier Corporation (2013).

[11] W. H. &. Y. A. W. Yeadon, J. McGraw− Hill Companies (2001).

[12] J. A. S. M. H. T. F. A. M.-F. J. I. R. &. D. J. Gomes, J. Journal of magnetism and magnetic materials 289 (2005) 184-187.

[13] V. K. C. P. B. S. S. M. P. V. S. V. N. S. &. N. S. V. Mittal, J. Solid state communications 137 (2006) 6-10.

[14] M. A.-A. S. M. T. A.-E. S. &. A.-E.-H. M. Amer, J. Turkish Journal of Physics 29 (2005) 163-177.

[15] B. N. C. L. M. &. H. J. M. Brockhouse, J. Physical Review 98 (1955) 1721.

[16] I. H. A. W. &. M. A. Gul, J. Journal of Magnetism and Magnetic Materials 320 (2008) 270-275.

[17] M. A. &. A. A. Y. M. abal, J. Materials Chemistry and Physics 118 (2009) 153-160.

[18] Y. L. J. W. Y. G. L. C. Y. Y. H. &. X. D. Lei, J. ACS applied materials & interfaces 6 (2014) 1773-1780.

[19] Y. F. H. R. G. X. C. &. T. J. M. Yang, J. ACS nano 8 (2014) 9518-9523.

[20] F. Z. D. &. C. Q. Zheng, J. ACS applied materials & interfaces 6 (2014) 9256-9264.

[21] Z. Z. Q. C. S. C. &. C. D. Yin, J. ACS Applied Materials & Interfaces 5 (2013) 9015-9025.

[22] V. S. P. &. D. B. Augustyn, J. Energy & Environmental Science 7 (2014) 1597-1614.

[23] H. G. S. S. N. W. C. &. W. Z. Zhang, J. RSC advances 4(59) (2014) 31328-31332.

[24] Y. C. Q. H. M. W. Y. S. X. X. H. &. W. X. Fu, J. Industrial & engineering chemistry research 51 (2012) 11700-11709.

[25] P. S. T. P. P. I. A. R. &. P. M. N. Samoila, J. Materials Chemistry and Physics 136 (2012) 241-246.

[26] A. D. A. B. A. N. V. I. A. &. P. M. Druc, J. Open Chemistry 11 (2013) 1330-1342.

[27] S. E. M. M. L. Y. Y. L. X. &. M. A. Shirsath, J. Journal of nanoparticle research 15 (2013).

[28] N. H. G. M. J. M. B. Y. Y. J. &. R. M. Sulaiman, J. Bio-medical materials and engineering 26 (2015) 103-110.

[29] V. G. M. J. B. D. A. &. N. K. S. Jeseentharani, J. Journal of experimental nanoscience 8 (2013) 358-370.

[30] K. C. J. T. &. R. K. Mouli, J. Journal of Nanoscience and Nanotechnology 9 (2009) 5596-5599.

[31] Ü. A. Y. &. M. H. Özgür, J. Journal of Materials Science: Materials in Electronics 20 (2009) 789-834.

[32] R. &. J. R. Dilip, J. Energy, Ecology and Environment 3 (2018) 237-241.

[33] S. I. W. A. M. A. M. A. D. A. S. &. M. B. E. M. Abdelsalama.

[34] M. G. &. S. S. C. Shalini, J. AIP Publishing LLC 1728 (2016).

[35] K. S. S. &. G. S. Chandra, J. ICAME (2008) 247-252.

[36] M. S. J. H. W. A. A. M. N. &. A. M. Ahmad, J. Modern Physics Letters B 33 (2019) 195-219.

[37] E. &. G. I. H. Pervaiz, J. Journal of magnetism and magnetic materials 324 (2012) 3695-3703.

[38] A. I. I. A. R. &. P. M. N. Borhan, J. Materials Research Bulletin 48 (2013) 2549-2556.

[39] T. S. A. T. &. V. T. George, J. Materials Science and Engineering 73 (2015) 12-50.

[40] M. C. K. H. A. P. P. J. &. S. R. Dimri, J. Journal of Magnetism and Magnetic Materials 486 (2019).

[41] M. A. I. A. S. K. M. M. G. A. I. &. I. M. Farid, J. Ovon Res 11 (2015) 1-10.

[42] M. D. N. T. M. R. &. H. A. A. Rahaman, J. Journal of Magnetism and Magnetic Materials 451 (2018) 391-406.

[43] A. A. S. S. S. Y. S. P. P. P. S. &. R. K. Y. Kadam, J. Journal of Magnetism and Magnetic materials 329 (2013) 59-64.

[44] M. Kaiser, J. Physica B: Condensed Matter 407 (2012) 606-613.

[45] N. K. V. &. S. S. K. Kumari, J. RSC Advances 5 (2015) 37925-37934.

[46] S. E. T. B. G. &. J. K. M. Shirsath, J. Materials Chemistry and Physics 117 (2009) 163-168.

[47] M. L. &. M. M. A. Levin, J. Uspekhi Fizicheskikh Nauk 135 (1981) 425-440.

[48] A. A. E. M. M. A. B. M. &. Z. S. H. Ali, J. Journal of Electrostatics 73 (2015) 12-18.

[49] R. S. S. F. C. M. K. R. M. D. M. A. S. &. S. F. S. M. Melo, J. Journal of Magnetism and Magnetic Materials 381 (2015) 109-115.

[50] W. M. Doyle, J. Process Control Qual 2 (1992) 11-41.

[51] P. R. &. D. H. J. A. Griffiths, J. John Wiley & Sons 171 (2007).

[52] X. S. X. C. Y. Z. D. &. M. Y. Zhang, J. Materials Letters 68 (2012) 336-339.

[53] N. M. &. A. A. Deraz, J. Electrochem 7 (2012) 4585-4595.

[54] A. A. A. S. M. &. M. T. M. El Ata, J. Solid State Sciences 6 (2004) 61-69.

[55] M. Z. G. I. H. &. M. A. Khan, J. Journal of Superconductivity and Novel Magnetism (2020) 1-12.

[56] R. D. Waldron, J. Physical review 99 (1995) 17-27.

[57] R. J. R. S. P. &. G. S. Dilip, J. Results in Materials 7 (2020).

[58] A. M. M. M. B. &. I. N. G. Wahba, J. Journal of Magnetism and Magnetic Materials 408 (2016) 51-59.

[59] M. L. &. M. M. A. Levin, J. Soviet Physics Uspekhi 24 (1981).

[60] A. S. P. &. V. D. Kumar, J. Ceramics International 40 (2014) 12855-12860.

[61] A. A. &. R. K. Y. Kadam, J. Journal of Materials Science: Materials in Electronics 27 (2016) 10484-10496.

[62] N. K. V. &. S. S. K. .. Kumari, J. RSC Advances 5 (2015) 37925-37934.

[63] M. Z. K. F. A. &. I. M. A. .. Ahsan, J. Results in Physics 14 (2019) 102-484.

[64] E. &. G. I. H. Pervaiz, J. Journal of magnetism and magnetic materials 349 (2014) 27-34.

[65] L. T. X. P. L. &. Z. X. Li, J. Journal of alloys and compounds 545 (2012) 67-69.

[66] A. &. S. M. S. Franco Jr, J. Journal of Applied Physics 109 (2011).

[67] R. &. A. N. H. Qindeel, J. Current Applied Physics 18 (2018) 519-525.

[68] S. I. W. A. M. A. M. A. D. A. S. &. M. B. E. M. Abdelsalama.

[69] A. G. T. C. M. R. G. &. K. P. Verma, J. Journal of Magnetism and Magnetic materials 208 (2000) 13-19.